THERMOMECHANICAL IDENTIFICATION OF A THRESHOLD IN THE CYCLIC RESPONSE OF "SFRP": FAST IDENTIFICATION OF THE FATIGUE PROPERTIES AND CORRELATION TO MICROSTRUCTURAL DATA

L. Jégou[12*], Y. Marco[1], V. Le Saux[1], S. Calloch[1]

[1]*Université Européenne de Bretagne, ENSTA Bretagne, Laboratoire Brestois de Mécanique et des Systèmes EA 4325, 2 rue François Verny 29806 Brest Cedex 9 France*
[2]*Université Européenne de Bretagne, IUT Saint-Brieuc (Université de Rennes1), Département Sciences et Génie des Matériaux, 18 rue Wallon BP406 22004 Saint-Brieuc Cedex*
**e-mail address of the corresponding author: loic.jegou@univ-rennes1.fr*

Keywords: Injection, SFRP, Heat build-up, X-ray micro-tomography

Abstract
Designing short fibers reinforced thermoplastics (SFRP) components is now a major concern for the automotive industry. This task is difficult because of the numerous factors affecting the fatigue lifetime coupled to long fatigue campaigns. To speed up the fatigue characterization, a 50% glass fibers reinforced polyamide 6,6 (PA66GF50) has been studied, using a heat build-up protocol developed for metallic materials. The life time estimation given by a first rough analysis is compared successfully to the fatigue curve obtained from a classical campaign. To understand what is caught from the thermal measurements, the evolution of the microstructure throughout the heat build-up test was investigated by X-ray micro-tomography and SEM and compared to the evolution of the mechanical features.

1 Introduction

Restricted a few years ago, to automotive applications with limited mechanical requirements, fibers reinforced thermoplastics (SFRP) are now used for structural components [1-4]. Designing those parts against fatigue has therefore become a serious issue over the last years, generating an extended literature [5-8]. Two main kinds of difficulties make this task complex. The first one is the nature of the matrix (usually PA66) because of the low glass temperature (around 70°C for a dry state) compared to the service temperature. This requires to use a rich constitutive law accounting for viscosity, plasticity, damage [9-10]. Moreover, the hydrophilic nature of this matrix inducing a decrease of the glass temperature [11] and consequently a drop of the fatigue properties under humid service conditions [7, 12]. The second main factor is the very strong coupling between the microstructure on the one hand and both the geometry and the process parameters on the other hand. The characterization of the influences of these numerous environment and process parameters on the fatigue properties therefore requires wide fatigue campaigns, which are even more time consuming than for metallic materials because these viscous materials exhibit a high heat build-up for fatigue tests lead at high frequencies [8]. It would therefore be very useful to speed up the characterization of the fatigue properties of these materials.

The aim of the project is therefore to investigate the relevancy of predicting the fatigue curve from heat build-up measurements for SFRP materials, as done recently on elastomers [15].

This paper details the experiments and the estimation given by a first rough analysis is compared to the fatigue curve obtained from a classical campaign. The agreement obtained is clearly good. A first development is to seek the identification of the dissipation sources, which is performed in a companion paper in this conference [21]. A second point, developed in this paper, is to investigate the micro-mechanisms at work during the tests. The evolution of the microstructure during the heat build-up test is described using X-ray micro-tomography. This experimental method provided the identification of fiber-depleted zones (FDZ) i.e. polyamide matrix, porosity or voids. These areas can be seen as fatigue initiation sites involving plasticity or damage under cyclic loading, as illustrated by the comparison to the mechanical indicators. Their geometrical evolution and their localization during the loading levels are illustrated with 3D pictures and 2D graphs. SEM observations have completed this investigation giving a very local view of damage (crack initiation and crack propagation) during a heat build-up test protocol. Based on these results, a scenario for fatigue damage evolution is proposed.

2 Materials and testing methods

2.1 Material and specimen

The material used here is a short glass fibers reinforced polyamide 6,6 containing 50% by weight (PA66-GF50). A standard tensile test specimen was used (geometry reported in Fig. 1). This geometry is defined in ISO 527-2-1A standard [36] and is classical for fatigue tests. The samples were injection moulded using a Billion 200T injection moulding machine and weighed immediately after moulding in order to master the subsequent water uptake. The specimens were conditioned in a humidity ratio kept at 40% and weighed before the tests to insure the same water content.

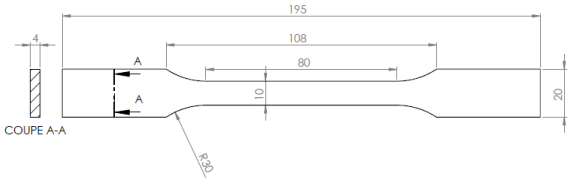

Figure 1. Sample geometry. The dimensions are given in mm

2.2 Mechanical testing and thermal measurements

2.2.1 Thermal measurements

The temperature measurements were performed with a MWIR 9705 FLIR infrared camera. This device is equipped with a Stirling-cycle cooled Indium-Antimonide (InSb) Focal Plane Array (FPA). The FPA is a 256x320 array of detectors digitized on 14 bits and sensitive in the 3-5µm spectral band. In order to convert the signal into a temperature (in °C), a preliminary calibration operation was achieved with a HGH DCN1000 N4 extended black body and a classical 2 points Non Uniformity Correction (NUC) was applied to the array of detectors. To minimize the influence of the external environment on the measurements, a "black box" surrounds the sample and the grips of the testing machine. After this calibration operation, a 20mK precision is obtained on relative measurements.

The temperature variation is computed from measurements performed on 3 zones. One located in the middle of the specimen (between the knives of the extensometer, called T) and the other two located on the upper and lower grips (respectively T^u and T^l). The temperature

variation is then calculated from the current set of temperatures (T, T_u, T_l) and from the initial temperatures (T_0, T^u_0, T^l_0) using the equation:

$$\theta = T - T_0 - \left[\frac{(T^u - T^u_0) + (T^l - T^l_0)}{2}\right] \quad (1)$$

This permits to avoid any artifact induced by the evolution of the ambient temperature or the servo-hydraulic machine.

2.2.2 Heat build-up protocol

A heat build-up experiment can be defined as a succession of cyclic tests of increasing stress or strain amplitude while the temperature of the specimen is measured. The number of cycles used for each loading condition is the number of cycles needed for the temperature to stabilize (for example, 2000 cycles at 1 Hz are sufficient for the samples used). These tests were achieved at room temperature, on an INSTRON 1342 hydraulic machine, equipped with hydraulic grips. The frequency of the tests was 1 Hz in order to limit the heat build-up effect and the experiments were stress controlled. The temperatures of the specimens were measured by the infrared camera and the maximum rise of temperature encountered was 10°C. The strain is measured by an INSTRON extensometer (reference 2610-601, base length 12.5±5 mm). Between each cycling period of 2000 cycles, the sample is unloaded and a pause of 10 minutes is allowed, in order to let the sample cool down and to get back to thermal equilibrium with the ambient. This step is also used to evaluate the partial recovery of the strain reached at the end of the cyclic loading. Let us precise that the last loading step is left running till the failure of the specimen, giving a number of cycles to failure.

2.2.3 Fatigue tests

Fatigue tests were achieved at room temperature, on an INSTRON 1342 hydraulic machine, equipped with hydraulic grips. The frequency of the tests was 1 Hz in order to limit the heat build-up effect and the experiments were stress controlled. The maximum rise of temperature encountered for high amplitudes was 10°C. This value and the limited number of cycles should limit any coupled thermal or chemical effect during the test. The load ratio was set to R=0. As commonly observed [19], the propagation step is very quick, allowing using the number of cycles leading to failure as the initiation lifetime.

3 Results and first analysis of the heat build-up curve

3.1 Heat build-up curve and first analysis

Figure 2a shows a typical result obtained for a loading step. A stabilization of the temperature increase was consistently observed (at the limited frequency imposed) and this stabilization means that the dissipation source is nearly constant: equilibrium between what is lost by conduction and convection and induced by cyclic loadings is reached.

Figure 2b presents the evolution of the stabilized temperature with respect to the stress amplitude imposed. On this chart, the results obtained from seven different tests are plotted. Test 1 and 2 played respectively 3 and 6 consecutive loading blocks. Tests 3 to 7 only played one single block. The very good correlation observed on the measured stabilized temperatures validates the reliability of the measurements and makes it clear that the thermal response obtained for one block is not much influenced by the former loading history.

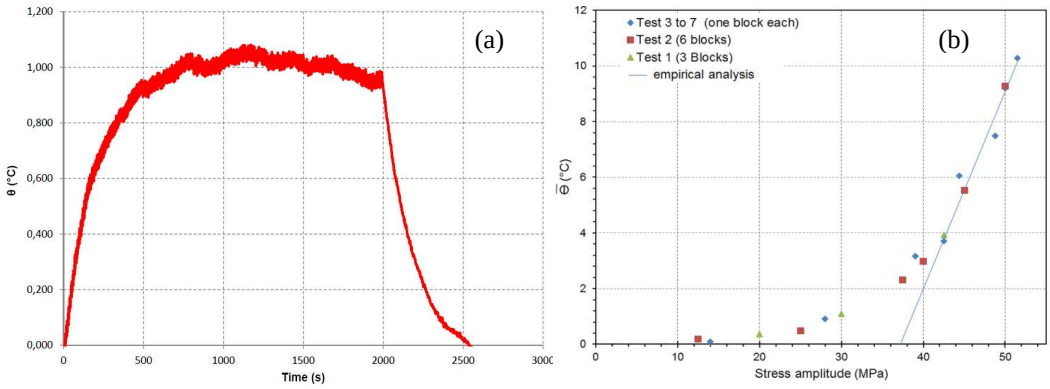

Figure 2. Evolution of the temperature along one loading step (a) and evolution of the stabilized temperature versus the applied stress amplitude (b).

A first empirical analysis, featured on figure 2b, can be proposed: a straight line is drawn from the last points and the intercept with the stress amplitude axis is considered. For ISO527 samples, this analysis gives a value of 37 MPa.

3.2 Comparison to fatigue result

3ure 4 presents the curve obtained from the classical fatigue campaign. It can be observed that the stress amplitude evaluated from heat build-up measurements is actually very close to the one leading to a lifetime of 10^6 cycles, which is relevant for most of the industrial applications. Nevertheless, evaluating only one point of the Wöhler curve is clearly not sufficient as the slopes of these curves may be quite different depending on conditioning or fibers orientation, for example [5,6,7]. This limitation can be overcome quite easily as the heat build-up test also provides a number of cycles to failure, obtained for the last stress amplitude (filled symbol in Figure 3). Taking advantage of the flat shape of the curve, the following protocol could therefore be suggested: identify the stress amplitude leading to 10^6 cycles from the graphical analysis and draw a straight line using the lifetime identified on the last loading block. This rough analysis actually provides an effective approximation of the fatigue curve.

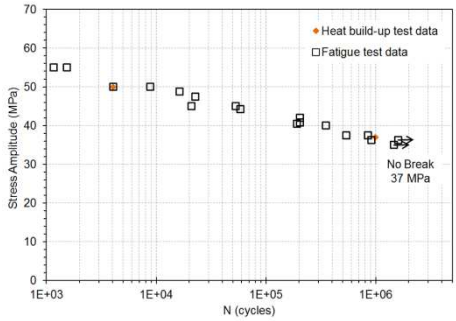

Figure 3. Fatigue curve obtained for IS0527 samples, R=0, frequency=1 Hz.

This kind of analysis is based on the idea that the stress amplitude evaluated can be seen as a threshold for the cyclic behavior of the material. Before comparing this value to the micro-structural evolution, it seemed therefore relevant to draw a comparison with the other classical mechanical parameters usually pointed out for fatigue, i.e. damage and plasticity. This comparison is performed on figure 4 and shows that the evolution of damage and permanent strain seems to support the idea of a change in the cyclic behavior, for a value close to the one evaluated from the temperature measurements.

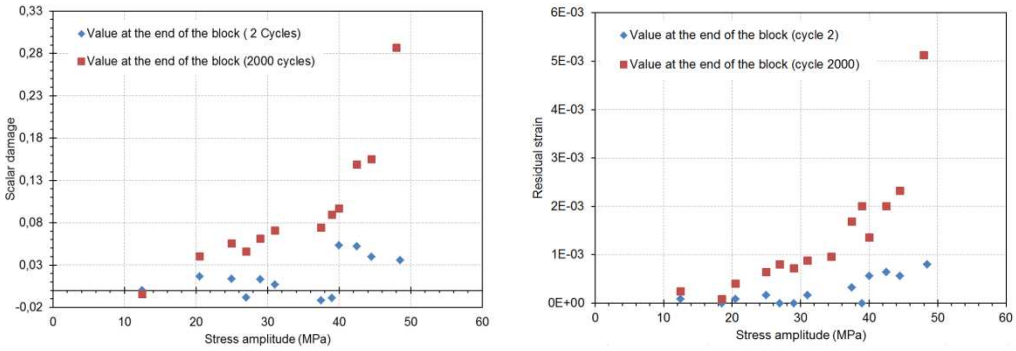

Figure 4. Evolution of damage and permanent strain during the heat built-up loading blocks.

4 Evolution of the microstructure throughout a loading step

4.1 X-ray micro-tomography

X-ray micro-tomography was used to identify the fatigue mechanisms on 5 specimens. Each sample has been submitted to a single loading block for 5 different stress amplitudes (2000 cycle at 13, 26, 39, 44 or 52MPa). X-Ray machine used is a V-TOME-X 240D. The resolution used (12µm) did not allow to isolate individual fibers and prevented from identifying clearly voids or porosities. It was therefore decided to observe the fiber-depleted zones (FDZ, abusively called "defects zones"), which were clearly likely to home the plasticity or damage occurrences. Three volumes located in the central area of the specimens (on Figure 5) have been investigated for each specimen.

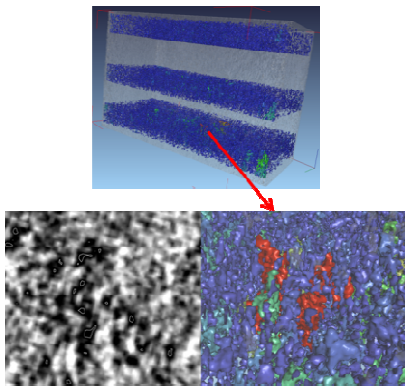

Figure 5. 3D view of a big and complex defect from X-ray micro-tomography measurement

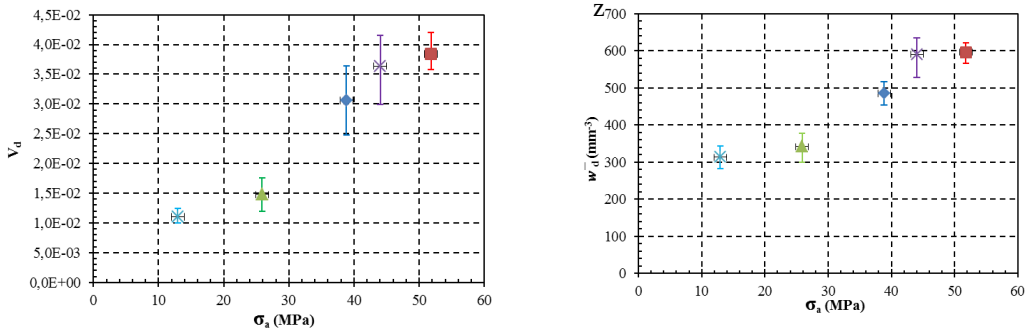

Figure 6. Evolution of the volume fraction and the defects density.

The measurements exposed the geometrical evolution of the microstructure and the localization of plasticity or damage initiation sites during the loading steps. Six parameters are defined: volume fraction of defects V_d; volume density of defects $\overline{w}_d$ [mm^{-3}]; volume of biggest defect $\mathbf{v}_{dmax}$ [mm^3]; average volume of an equivalent rectangular cuboid representing a defect v_{pme} [mm^3]; sum of the defects projections along the x-axis, y-axis and z-axis called

respectively $\sum P_X$, $\sum P_Y$ and $\sum P_Z$ [mm²]; defects locations with a volume greater than 100 voxels in a $(\vec{X}\,;\vec{Y})$ section (z-axis is the loading direction).

All these parameters clearly indicated an increase in the size and number of FDZ for a value slightly lower than 39Mpa (V_d and $\overline{w}_d$ on Figure 6). This confirms the existence of a threshold of the stress amplitude around 37Mpa. Figure 7 confirmed the geometrical anisotropy of FDZ which is consistent with respect to the flow direction and the loading direction. We also noticed an increase of the geometric anisotropy of the defects in the loading direction with the loading amplitude.

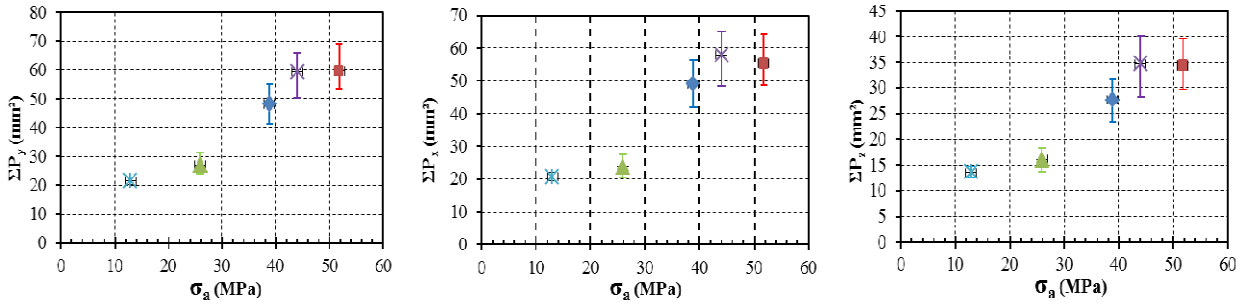

Figure 7. Evolution of the geometrical parameters during the loading steps of a heat build-up test.

Figure 8 presents the localization of the FDZ on a specimen section. A majority of defects appear in the heart and in the corners of the specimen. In addition, the number of defects increases sharply just before stress amplitude of 39MPa. These locations are also areas where the fibers are misaligned with respect to the loading direction, which facilitates the onset of plasticity or damage.

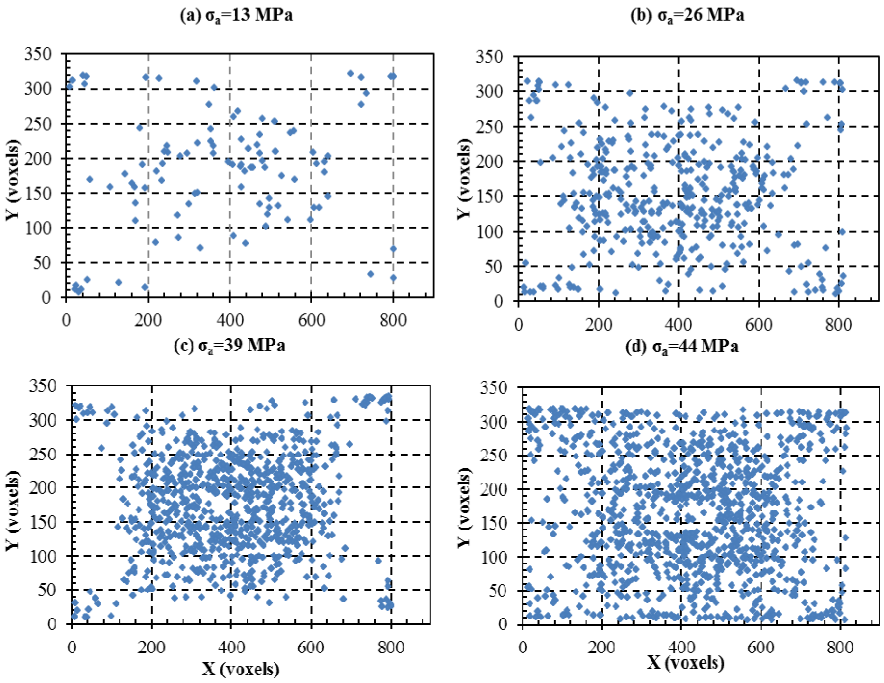

Figure 8. FDZ location during the loading steps of a heat build-up test (FDZ >100 voxels).

4.1 SEM observations

In order to help sorting damage from plasticity, SEM observations have been achieved. Many fibers appear broken and some are loosened from the polymer matrix (on Figure 9 (c)), especially for the highest stress amplitude (2000 cycles for 52 MPa). Nevertheless, spherical

cavities were observed within the matrix of the samples whatever the stress level imposed (see Figure 9 (a)) and it is difficult to offer a privileged location for this phenomenon. The size of these porosities (from 0.5µm to 5µm see Figure 9 (b)) and their very low density barely explained the clear evolution observed on the mechanical indicators. These porosities seems therefore induced by the injection process rather than by the mechanical loading (except for the highest level).

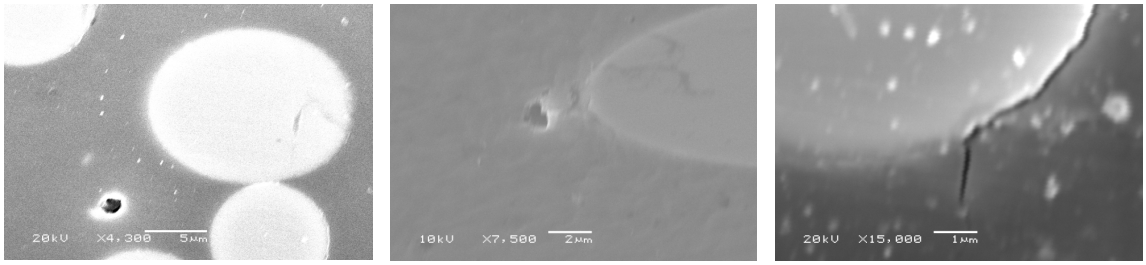

(a) (b) (c)

Figure 9. SEM observations of PA66GF50: (a) spherical cavities; (b) cavities near a fiber; (c) debonding and crack around a fiber.

Coupled to the previous X-ray observations, these observations reveals that the identification of the fatigue sites and mechanisms is not an easy task and it seems that plasticity at low scales play a higher role than damage, which is the usual explanation.

4 Conclusions

This paper demonstrates that a rough yet pragmatic protocol based on the analysis of the heat build-up curve provides a very reasonable evaluation of the Wohler curve. This is an important result because it means that a fairly good identification of the fatigue curve could be achieved using only one sample with a test lasting less than 2 days (including the failure on the last heat build-up block). A deeper analysis is required in order to go provide a fatigue criterion, which is discussed in a companion paper [22]. This analysis is based on the hypothesis of a threshold, which is observed as well on mechanical indicators. SEM observations failed to reveal a similar damage evolution, which seems to be more dependent on the number of cycles than on the stress amplitude applied. X-ray tomography fails to dissociate plastic and damaged areas but showed a growth in size and number of areas with low fibers content, for a level correlated to the macroscopic indicators. It therefore seems interesting to investigate the fatigue behaviour with micro-plasticity in mind. Morevover, as the scale transition for fatigue mechanisms remains, difficult, a global indicator such as dissipated energy seems relevant.

References

[1] A. Bernasconi, P. Davoli, C. Armanni, *Fatigue strength of a clutch pedal made of reprocessed short glass fibre reinforced polyamide*, **International Journal of Fatigue 32**, 100-107, (2010)

[2] J. Casado, I. Carrascal, J. Polanco, F. Gutierrez-Solana, *Fatigue failure of short glass fibre reinforced PA 6.6 structural pieces for railway track fasteners*, **Engineering Failure Analysis 13**, 182-197, (2006)

[3] L. Jegou, Y. Marco, S. Calloch, C. Doudard, *Evaluation of the influence of geometrical and injection parameters on the fatigue life of PA66GF50 based on heat build-up measurements*, **Procedia Engineering 2**, 1741-1750, (2010)

[4] C. Sonsino, E. Moosbrugger, *Fatigue design of highly loaded short-glassfibre reinforced polyamide parts in engine compartments*, **International Journal of Fatigue 30**, 1279-1288, (2008).

[5] J. Horst, J. Spoormaker, *Mechanisms of fatigue in short glass fiber reinforced polyamide 6*, **Polymer Engineering and Science 36,** 2718-2726, (1996).
[6] A. Bernasconi, P. Davoli, A. Basile, A. Filippi, *Effect of fiber orientation on the fatigue behaviour of a short glass fiber reinforced polyamide-6*, **International Journal of Fatigue 29,** 199-208, (2007).
[7] A. Bernasconi, P. Davoli, D. Rossin, C. Armanni, *Effect of reprocessing on the fatigue strengh of a fiberglass reinforced polyamide*, **Composites Part A 38,** 710-718, (2007)
[8] A. Bernasconi, R. Kulin, *Effect of frequency upon fatigue strengh of a shot glass fiber reinforced polyamide 6: a superposition method based on cyclic creep parameters*, **Polymer Composites 30,** 154-161, (2008).
[9] A. Andriyana, N. Billon, L. Silva, *Mechanical response of a short fiber reinforced thermoplastics: experimental investigations and continuum mechanical modeling*, **European Journal of Mechanics - A/Solids 29**, 1065-1077 (2010).
[10] A. Launay, M. Maitournam, Y. Marco, I. Raoult, F. Szmytka, *Cyclic behaviour of short glass fiber reinforced polyamide: experimental study and constitutive equations*, **International Journal of Plasticity 27**, 1267–1293, (2011).
[11] K. Reimschluessel, *Relationships of the effect of water on glass transition temperature and Young's modulus of nylon 6*, **Journal of Polymer Science**: Polymer Chemistry Edition 16, 1229-1236 (1978).
[12] S. Barbouchi, V. Bellenger, A. Tcharkhtchi, P. Castang, T. Jollivet, *Effect of water on the fatigue behaviour of PA66/glass fibers composite materials*, **Journal of Materials Science 42,** 2181-2188, (2007).
[13] W. Herman, R. Hertzberg, J. Manson, *The influence of loading history on fatigue in engineering plastics*, **Journal of Materials Science 25,** 434-440, (1990).
[14] A. Zago, G. Springer, *Constant amplitude fatigue of short glass and carbon fiber reinforced thermoplastics*, **Journal of Reinforced Plastics and Composites 20,** 564.
23, (2001)
[15] R. Munier, C. Doudard, S. Calloch, B. Weber, *Towards a faster determination of high cycle fatigue properties taking into account a plastic prestrain from self-heating measurements*, **Procedia Engineering 2,** 1741-1750, (2010).
[16] M. Poncelet, C. Doudard, S. Calloch, B. Weber, F. Hild, *Probabilistic multiscale models and measurements of self-heating under multiaxial high cycle fatigue*, **Journal of the mechanics and Physics of Solids 58,** 578-593, (2010).
[17] V. Le Saux, Y. Marco, S. Calloch, C. Doudard, P. Charrier, *Fast evaluation of the fatiue lifetime of rubber-like materials based on a heat build-up protocol and micro-tomography measurements*, **International Journal of Fatigue 32,** 1582-1590, (2010).
[18] K. Noda, A. Takahara, T. Kajiyama, *Fatigue failure mechanisms of short glass-fiber reinforced nylon 66 based on nonlinear dynamic viscoelastic measurements*, **Polymer 42,** 5803–5811.24, (2001).
[19] A. Berrehili, Y. Nadot, S. Castagnet, J. Grandidier, C. Dumas, *Multiaxial fatigue criterion for polypropylene for automotive applications*, **International Journal of Fatigue 32,** 1389-1392, (2010).
[20] AFNOR, Plastiques – *Détermination des propriétés en traction*. **Norme Européenne, norme française (ISO 527-2)**, (1996).
[21] C. Doudard, S. Calloch, P. Cugy, A. Galtier, F. Hild, *A probabilistic twoscale model for high-cycle fatigue life prediction*, **Fatigue and Fracture of Engineering Materials and Structures 28,** 279-288, (2005).
[22] Y. Marco, L. Jégou, S. Calloch, Heat built-up measurements and energetic criterion used to evaluate quickly the fatigue life of PA66, in "Proceeding of **ECCM 15,** Venice, Italy (2012).